Electric and Optical Properties of Pb(Er$_{1/2}$Nb$_{1/2}$)-Pb(Mg$_{1/3}$Nb$_{1/3}$)-PbTiO$_3$ Crystals

Wei Zhao [1,2]**, Zengzhe Xi** [1,2,]*****, Pinyang Fang** [1,2]**, Xiaojuan Li** [1,2]**, Wei Long** [1,2]**, Aiguo He** [1,2]**,
Ying Li** [1,2] **and Yuanmin Zhang** [3]

[1]   Shaanxi Key Laboratory of Photoelectric Functional Materials and Devices, Xi'an 710021, China;
      zwxatu@163.com (W.Z.); fpy_2000@163.com (P.F.); lixiaojuan28@163.com (X.L.); longwei@xatu.com (W.L.);
      5129226701@163.com (A.H.); ly1436020975@163.com (Y.L.)
[2]   School of Materials and Chemical Engineering, Xi'an Technological University, Xi'an 710021, China
[3]   School of General Education, Xi'an University of Technological Information, Xi'an 710299, China;
      18009299092@163.com
*****   Correspondence: zzhxi@xatu.edu.cn; Tel.: +86-29-8617-3324

check for updates

Abstract: New ferroelectric crystals Pb(Er$_{1/2}$Nb$_{1/2}$)-Pb(Mg$_{1/3}$Nb$_{1/3}$)O-PbTiO$_3$ (PEN-PMN-PT) were grown by using the flux method. Phase structure of the crystals was described by the X-ray diffraction analysis. Dielectric, ferroelectric and optical properties of the PEN-PMN-PT crystals were investigated systematically. Higher Curie temperature (T_c ~291 °C) and larger coercive field (E_c ~17.6 kV/cm) for the 40PEN-13PMN-47PT can be obtained, respectively, compared with those of the PMN-PT. Moreover, strong green and red emissions can be excited by using the 980 nm laser. The PEN-PMN-PT crystals with these performances have some promising applications in the electromechanical and optical devices.

Keywords: Pb(Er$_{1/2}$Nb$_{1/2}$)-Pb(Mg$_{1/3}$Nb$_{1/3}$)O-PbTiO$_3$; electric and optical properties; Perovskite structure; UC emission mechanisms

1. Introduction

As a typical relaxor ferroelectric crystal, Pb(Mg$_{1/3}$Nb$_{2/3}$)O$_3$-PbTiO$_3$ (PMN-PT) with morphotropic phase boundary (MPB) composition has been extensively researched due to their excellent dielectric, piezoelectric and pyroelectric properties, such as ultrahigh piezoelectric coefficient (d_{33} > 1800 pC/N), high longitudinal electromechanical coupling factor (k_{33} > 90%), high dielectric constant (ε' > 4000) and low dielectric loss ($tan\delta$ < 0.01) et al. [1–5]. These brilliant properties make it good candidates in the applications of medical ultrasonic probes, underwater acoustic transducers, ultrasonic motors and military sensors [6].

However, PMN-PT show low coercive field (E_c < 3 kV/cm) and low Curie temperature (T_c < 150 °C), which gradually limit their applications in high temperature and high energy fields [7]. In order to raise the Curie temperature and coercive field of the PMN-PT crystals, a lot of researches and trials have been done [7–15]. Luo et al. [16] reported that the E_c and T_c of Mn-doped PMN-29PT crystals increased by 1.65 kV/cm and 15 °C, respectively. Li et al. [17] explored new ternary crystals Pb(Ho$_{1/2}$Nb$_{1/2}$)O$_3$-Pb(Mg$_{1/3}$Nb$_{2/3}$)O$_3$-PbTiO$_3$ (PHN-PMN-PT) with the E_c and T_c of 3.22 kV/cm and 140 °C, respectively. The E_c ~8.17 kV/cm and T_c ~148 °C were achieved in 6PSN-63PMN-31PT by He et al. [18]. These results indicate that the Curie temperature and coercive field of the PMN-PT crystals can be improved with the appropriate cations.

Previous reports indicated that Curie temperature and coercive field of the PMN-PT crystals can be improved by the rare earth cation of Erbium [19]. In addition, high Curie temperature can be

obtained in the Pb(Er$_{1/2}$Nb$_{1/2}$) (PEN) ceramics [20]. In the present work, the PEN was used to modify PMN-PT crystals by using the linear design rule on the component of the PEN-PMN-PT crystals. The structural, electrical and optical properties of the PEN-PMN-PT crystals were studied systematically.

2. Experimental Procedure

2.1. Crystal Growth

The 20PEN-40PMN-40PT and 40PEN-13PMN-47PT were chosen on the straight line connecting two MPBs in PMN-33PT and Pb(Er$_{1/2}$Nb$_{1/2}$)-50PbTiO$_3$ (PEN-50PT), as shown in Figure 1 [7,21]. The crystals of two components were grown by using the flux method. First of all, the starting materials of MgO (99.99%), Nb$_2$O$_5$ (99.99%), TiO$_2$ (99.99%), PbO (99.99%) and Er$_2$O$_3$ (99.99%) were prepared, and the precursors, MgNb$_2$O$_6$ (MN) and ErNbO$_4$ (EN) were first synthesized at 1050 °C for 6 h. MN, EN, TiO$_2$ and PbO were weighed according to the stoichiometric composition of the 20PEN-40PMN-40PT and 40PEN-13PMN-47PT, with 60 *wt*% excess amount of PbO, and then the raw materials were mixed and wet-milled in alcohol for 12 h. The dried mixed powder was compacted in a platinum crucible with a size of Φ 40 mm × 40 mm and covered with a platinum lid. The platinum crucible was then placed in a corundum crucible, and filled with Al$_2$O$_3$ powder in the gap. After that corundum crucible was placed in the high temperature furnace and crystal growth was performed according to the preset procedure. At the end of crystal growth, the Pt crucible was taken out and was boiled with hot nitric acid solution (mixture of HNO$_3$ and H$_2$O with a volume ratio 1:1). Finally, the obtained crystal was cleaned in the CNC ultrasonic cleaner (KQ-100DE).
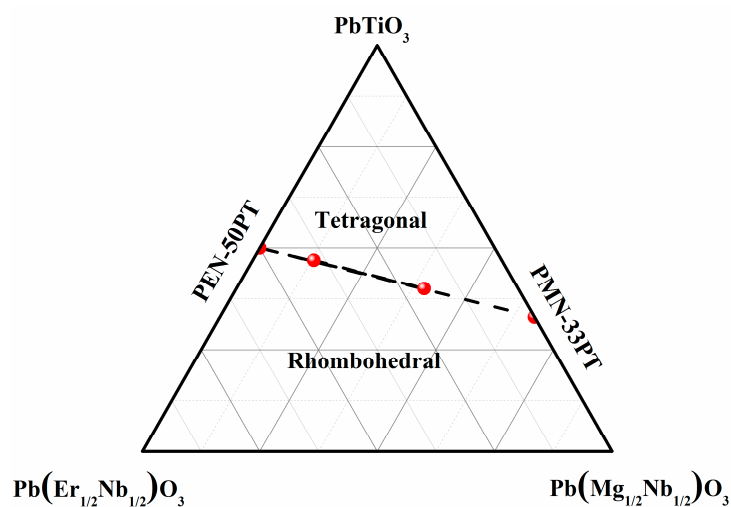

**Figure 1.** Phase diagram of PEN-PMN-PT ternary system.

2.2. Characterization Procedure

Firstly, the phase structure of the present crystals was measured by X-ray diffraction (XRD) analysis (D8 ADVANCE, Bruker, Billerica, MA, USA) with Cu-Ka radiation, perating at room temperature in a scan steps of 0.02 (2θ) and an angular range of 20–80°. Secondly, the crystals were polished for the two parallel surfaces, and then polished crystals were coated with silver paste on both polished surfaces and fired at 550 °C for 30 min to obtain the electrode. Eventually, the temperature dependence of dielectric properties was measured by impedance analyzer (Agilent4294A, Agilent, Santa Clara, CA, USA). The ferroelectric performances of the samples were tested by using ferroelectric test system (Radiant Precision Premier II, Radiant Technologies, Inc., Albuquerque, NM, USA). The optical absorption performances of crystal powders were measured by UV-VIS-NIR Spectrophotometer (UV3600PLUS, Shimadzu, Japan). The up-conversion (UC) photoluminescence

(PL) and decay curve of the 20PEN-40PMN-40PT and 40PEN-13PMN-47PT crystals were tested by using a photoluminescence spectrometry (FLS980, Edinburgh, England) at room temperature.

3. Results and Discussion

XRD patterns of the powders and natural exposure surfaces of the PEN-PMN-PT crystals are shown in Figure 2. In Figure 2a, the positions and intensity of the main diffraction peaks are consistent with those of the $Pb(Mg_{1/3}Nb_{2/3})O_3$ (PDF#81-0861). No obvious diffraction peaks of the secondary phases are detected, indicating that the phase structure of the present crystals is pure perovskite structure. The natural exposure surfaces of the present crystals are shown in Figure 2b,c. Only three diffraction peaks of the (100), (200) and (300) can be detected, which indicate that the natural exposure surface of the present crystals is strict {100} surface and the slowest growth direction is [100] orientation. Moreover, the (200) peak at around $2\theta = 45°$ is an important differential characteristic peak, which is used to determine the MPB compositions. It is well-know that only one characteristic peak R(200) can be observed at around $2\theta = 45°$ for rhombohedral phase, whereas (200) peak should be split into two peaks with intensity ratio of 1:2 for tetragonal phase. They correspond to the diffraction of $T(200)/(020)$ and $T(002)$, respectively [10]. Obvious splitting of the (200) peak with the deviated intensity ratio 1:2 can be observed in Figure 2, indicating that the tetragonal and rhombohedral phase coexist in the present crystals.
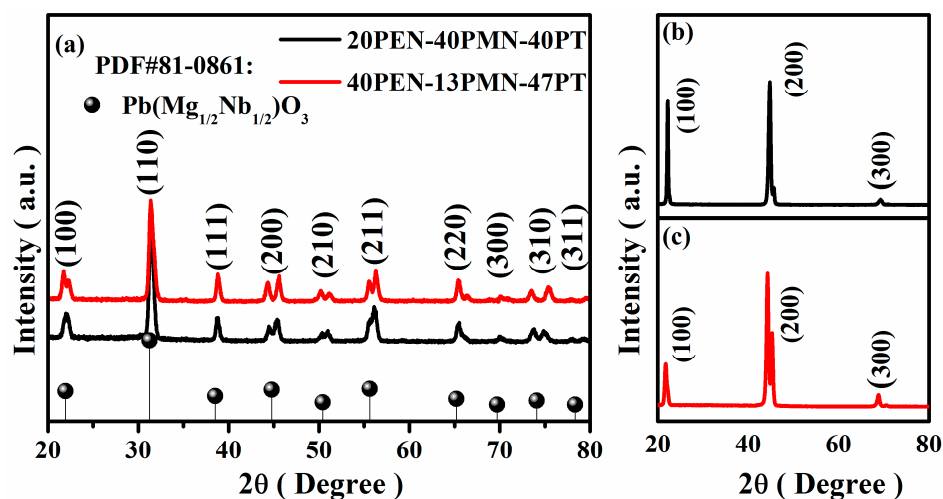

Figure 2. XRD patterns of (**a**) PEN-PMN-PT crystals powders; (**b**) [100]-oriented 20PEN-40PMN-40PT crystals; and (**c**) the [100]-oriented 40PEN-13PMN-47PT crystals.

In order to figure out the effect of the content of rhombohedral and tetragonal phases on electrical properties, the ratio of rhombohedral and tetragonal phase is calculated by the following equation [11]:

$$R/T = \frac{I_R(200)}{I_T(200) + I_T(002)} \tag{1}$$

where $I_R(200)$ is the intensity of the rhombohedral (200) peaks. $I_T(200)$ and $I_T(002)$ are the intensities of tetragonal (200) and (002) peaks. The XRD patterns fitted with the Gaussian functions are shown in Figure 3. Pink circles represent the fitted peak profile, and the green line and the blue line represent the deconvoluted profiles of the rhombohedral and tetragonal phase components, respectively. It is observed that the (200) reflection is composed of three reflection peaks of $T(200)/(020)$, $T(002)$ and $R(200)$. According to calculation, the ratio of rhombohedral and tetragonal phases is obtained to be 0.12 and 0.07 for the 20PEN-40PMN-40PT and 40PEN-13PMN-47PT, respectively. These results confirm that the tetragonal phase is dominant in the present crystals and higher content of the tetragonal phases could be responsible for the higher coercive filed [22].
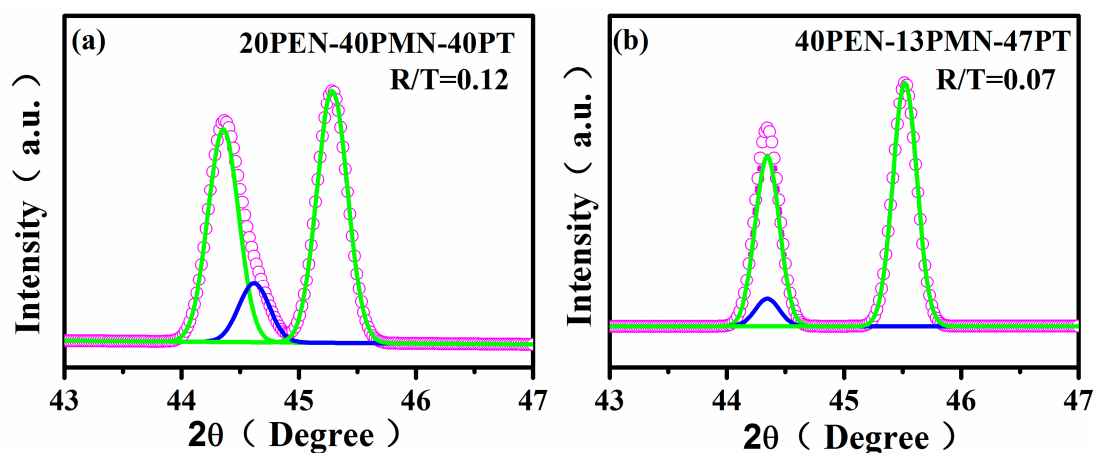
Figure 3. X-ray diffraction patterns fitted with Gaussian functions for (200) peaks at $2\theta = 43\text{–}47°$: (**a**) 20PEN-40PMN-40PT; (**b**) 40PEN-13PMN-47PT.

Temperature dependence of the dielectric permittivity of the unpoled PEN-PMN-PT crystals are shown in Figure 4. Only one dielectric peak, corresponding to the transition from ferroelectric to paraelectric phase, is observed for the present crystals. Curie temperatures are 207 and 291 °C for the 20PEN-40PMN-40PT and 40PEN-13PMN-47PT crystals. It indicates that the Curie temperature of the PMN-PT crystal can be improved significantly by the modification of the PEN. The reason for the improvement of Curie temperature of the present crystals is attributed to the introduction of the PEN. When PEN is incorporated into the PMN-PT system, relatively larger Er^{3+} substitutes are located at the B site. This will result in the decreasing of the perovskite tolerance means the rhombohedral or tetragonal phases become more stable. That leads to the increasing of the T_c [7]. Moreover, Curie temperature of PEN-PMN-PT crystals increases with the increase in the PEN and PT content, which is consistent with the results of the PYbN-PMN-PT crystals and PSN-PMN-PT ceramics [11,23].
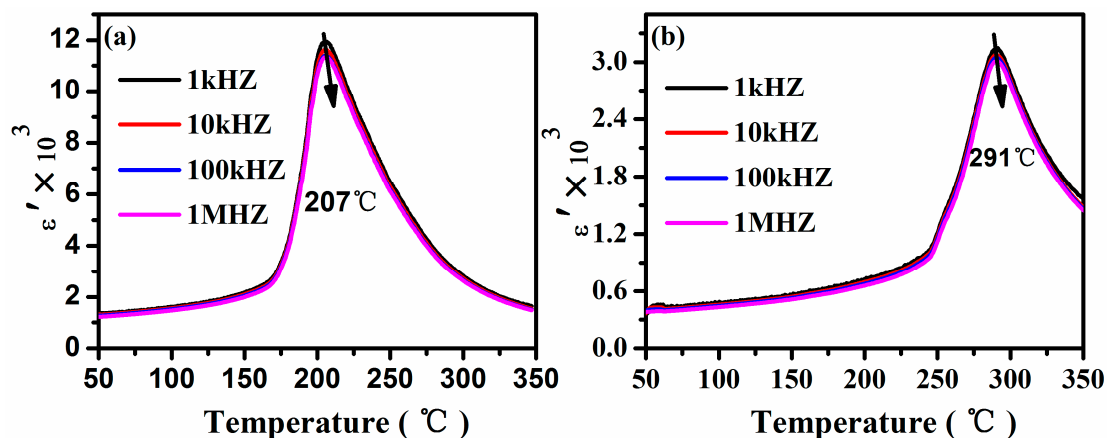
Figure 4. Temperature dependence of dielectric permittivity ε' for [100]-oriented PEN-PMN-PT: (**a**) 20PEN-40PMN-40PT; (**b**) 40PEN-13PMN-47PT.

Polarization versus electric field (*P-E*) of [100]-oriented PEN-PMN-PT crystals with 28 kV/cm at room temperature is shown in Figure 5. Higher coercive electric (E_c ~12.3 kV/cm and 17.6 kV/cm) and remnant polarization (P_r ~30 μC/cm^2 and 18.2 μC/cm^2) can be obtained for the 20PEN-40PMN-40PT and 40PEN-13PMN-47PT crystals compared with those of the PMN-PT crystal. In the present crystals, $Pb(Er_{1/2}Nb_{1/2})$ is incorporated into the PMN-PT system. Oxygen vacancies will be generated for the charge compensation when the Er^{3+} substitutes Ti^{4+} or $(Mg_{1/3}Nb_{2/3})^{4+}$ locates at B sites. The higher coercive filed of the present crystals is attributed to the domain motion prevented by the oxygen vacancies. The results are similar to those of the Er^{3+} doped PMN-PT and PSN-PMN-PT crystals [18,19].

Moreover, previous reports indicated that coercive filed of PZN-PYN-PT ceramic in MPB regions is mainly dependent on the tetragonal phase and have been improved with increasing of content of the tetragonal phase [22]. As a result, it is believed that the ratio of the rhombohedral and tetragonal phases in the present crystals is the reason of the difference of ferroelectric properties.
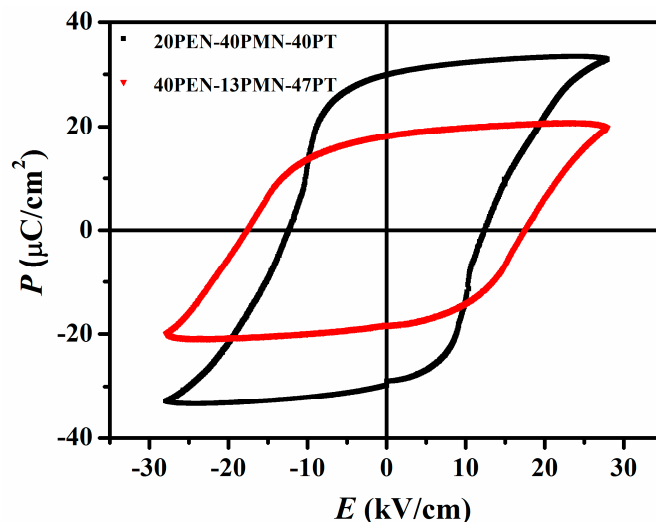
Figure 5. Ferroelectric hysteresis loop of [100]-oriented PEN-PMN-PT: crystal: (**a**) 20PEN-40PMN-40PT; (**b**) 40PEN-13PMN-47PT.

The UV–VIS–NIR absorption spectra of the PEN-PMN-PT crystals in the wavelength range of 400–1800 nm is shown in Figure 6. It can be seen that there are seven absorption peaks at around 489, 526, 665, 794, 974, 1467 and 1540 nm, corresponding to the Er^{3+} transitions from ground state $^4I_{15/2}$ to excited levels $^4F_{7/2}$, $^2H_{11/2}$, $^4F_{9/2}$, $^4I_{9/2}$, $^4I_{11/2}$ and $^4I_{11/2}$, respectively. It indicates that the optical absorption is induced by the rare earth cation of the Er^{3+} ions [11,19,24]. The absorption spectra of the PEN-PMN-PT crystals is similar as other Er^{3+}-doped ferroelectric materials [25,26].
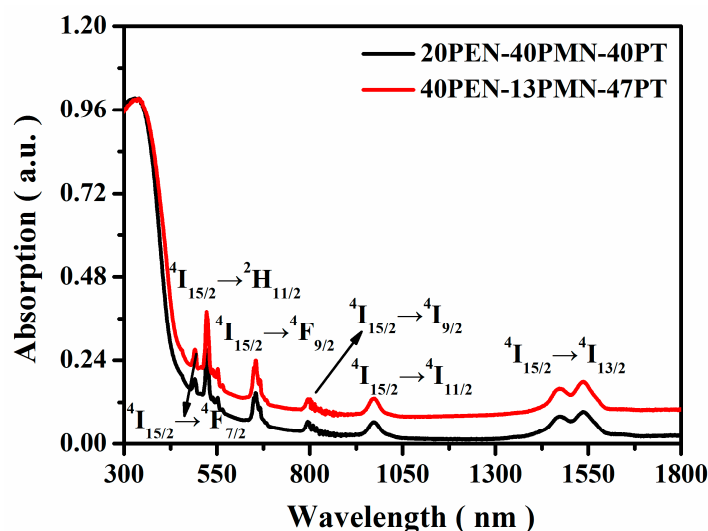
Figure 6. The UV–VIS–NIR absorption of PEN-PMN-PT crystals.

Figure 7 displays the UC luminescence of the PEN-PMN-PT crystals at room temperature. Under the excitation of 980 nm, three distinct emission bands, centered at 526 (green), 565 (green), and 665 nm (red), and the transition emissions' counterparts, $^2H_{11/2} \rightarrow {}^4I_{15/2}$, $^4S_{3/2} \rightarrow {}^4I_{15/2}$ and $^4F_{9/2} \rightarrow {}^4I_{15/2}$, are observed in the present crystals. The emission intensity at 665 nm is pretty much constant.

However, the obvious difference in luminous intensity at 565 and 526 nm can be observed as well. It may be related to different mechanisms in two crystals.
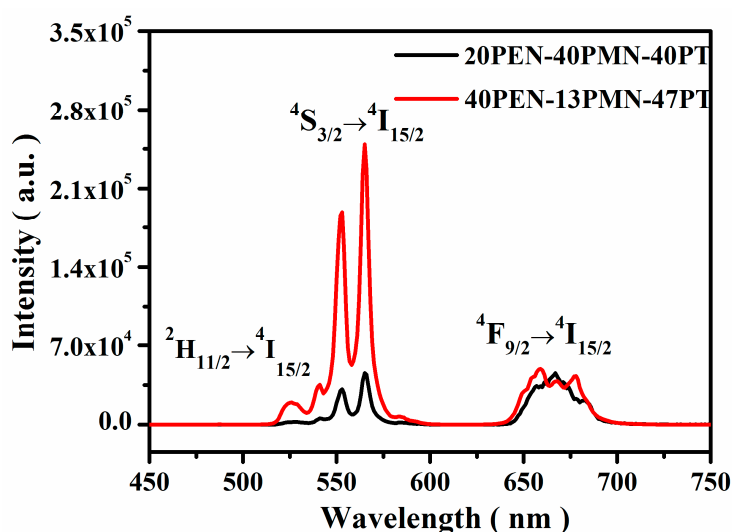

Figure 7. The UC emission spectra of the PEN-PMN-PT crystals under 980 nm excitation.

To study differences in luminous intensity at 565 and 526 nm in two crystals, the UC emission mechanisms is described in detail. Figure 8 shows the energy level diagrams and possible UC PL mechanisms of the PEN-PMN-PT crystals under 980 nm excitation. Er^{3+} ions are excited from the ground state $^4I_{15/2}$ to the excited state $^4I_{11/2}$ through the ground state absorption (GSA) process. Then, the Er^{3+} ions in $^4I_{11/2}$ energy level can reach a higher excited state $^4F_{7/2}$ through excited state absorption process (ESA) and the energy transfer (ET) process: $^4I_{11/2} + {}^4I_{11/2} \rightarrow {}^4I_{15/2} + {}^4F_{7/2}$. The Er^{3+} ions are unstable in $^4F_{7/2}$ level, which reach to $^2H_{11/2}$, $^4S_{3/2}$ and $^4F_{9/2}$ level by nonradiative transition process. Finally, the Er^{3+} ions return to the ground state $^4I_{15/2}$ with 526 (green), 565 (green) and 665 nm (red) emitted, respectively. Previous reports indicate the ET processes is enhanced with increasing Er^{3+} ions concentration because of short distance between neighboring Er^{3+} ions [26]. Therefore, Green emissions being significantly enhanced can be explained by the intense ET process that led to populated $^4I_{11/2}$ state.
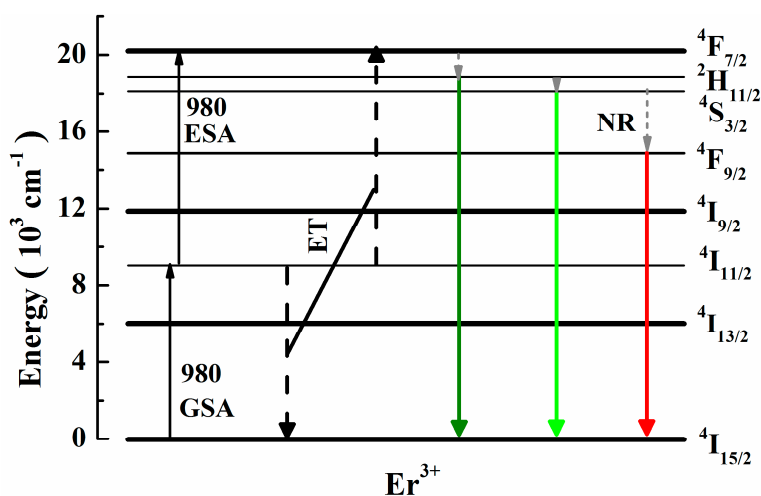

Figure 8. Schematic energy-level diagram of Er^{3+} ions in PEN-PMN-PT and up-conversion process.

The lifetime τ of energy level is an important parameter for the luminescent materials. The decay curves of $^4S_{3/2}$ and $^4F_{9/2}$ levels for the PEN-PMN-PT are shown in Figure 9. The double and triple

exponential function (2) is used to fit measured curves [27]. Equation (3) is used to calculate the average lifetimes τ_m.

$$I_{(t)} = I_0 * [A + B_1 \exp(-t/\tau_1) + B_2 \exp(-t/\tau_2) + B_3 \exp(-t/\tau_3)] \tag{2}$$

$$\tau_m = (B_1 \tau_1{}^2 + B_2 \tau_2{}^2 + B_3 \tau_3{}^2)/(B_1 \tau_1 + B_2 \tau_2 + B_3 \tau_3) \tag{3}$$

where A, B_1, B_2 and B_3 are constant, $I(t)$ is the emission intensity. All curves (black line) increase first and then decrease, standing for absorbing energy and releasing energy of electrons populating at ground state and excited state, respectively. The fitting curve (red line) matches perfectly with the measured curve. The lifetimes of 20PEN-40PMN-40PT crystals exhibit a triple exponential decaying behavior, but the 40PEN-13PMN-47PT crystals display a double exponential behavior. Fitting results of fluorescent decay curve for the present crystals are shown in Table 1. The average lifetime of $^4S_{3/2}$ level in 40PEN-13PMN-47PT crystals increases (44.00 us) compared with that of 20PEN-40PMN-40PT crystals (45.57 us). However, the average lifetime of $^4F_{9/2}$ decreases with the increase of the concentration Er^{3+} ions. The increase of Er^{3+} concentration enhances energy transfer (ET) process. The intense ET process makes the $^4F_{9/2}$ excited levels become populated, resulting in the population of $^4S_{3/2}$. Ultimately, the enhanced process $4S_{3/2} \rightarrow {}^4I_{15/2}$ leads to the average lifetime increase from 44.00 to 45.57 us. Nevertheless, owing to the depopulation of the $^4I_{15/2}$ level, the possibility of the $^4F_{9/2} \rightarrow {}^4I_{15/2}$ transition will decrease, resulting in the average lifetime of $^4F_{9/2}$ from 105.79 to 69.60 us.
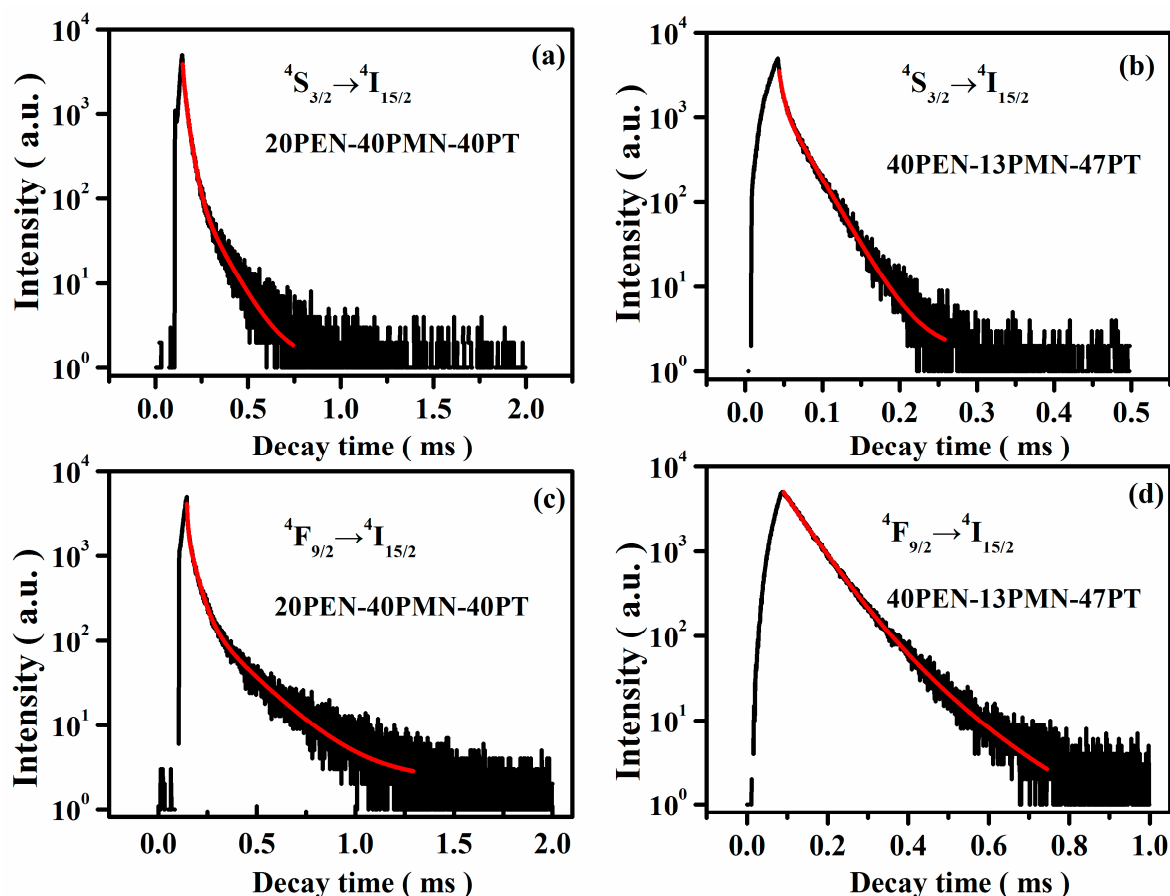
Figure 9. Emission lifetime of PEN-PMN-PT crystals under 980 nm excitation (**a**) 20PEN-40PMN-40PT crystals at 526 nm ($^4S_{3/2} \rightarrow {}^4I_{15/2}$); (**b**) 40PEN-13PMN-47PT crystals at 526 nm ($^4S_{3/2} \rightarrow {}^4I_{15/2}$); (**c**) 20PEN-40PMN-40PT at 667 nm ($^4F_{9/2} \rightarrow {}^4I_{15/2}$); (**d**) 40PEN-13PMN-47PT at 667 nm ($^4F_{9/2} \rightarrow {}^4I_{15/2}$).

Table 1. Fitting results of fluorescent decay curve for the PEN-PMN-PT crystals.

Samples	$^4S_{3/2} \rightarrow {}^4I_{15/2}$				$^4F_{9/2} \rightarrow {}^4I_{15/2}$			
	τ_1	τ_2	τ_3	τ_m	τ_1	τ_2	τ_3	τ_m
20PEN-40PMN-40PT	6.93	33.75	90.15	44.00	13.91	33.24	177.23	105.79
40PEN-13PMN-47PT	9.84	55.57		45.57	59.07	118.97		69.60

4. Conclusions

New ferroelectric crystals $Pb(Er_{1/2}Nb_{1/2})$-$Pb(Mg_{1/3}Nb_{1/3})O$-$PbTiO_3$ (PEN-PMN-PT) were grown by using the flux method. Pure perovskite structure was confirmed by X-ray diffraction analysis. Dielectric and ferroelectric properties were improved significantly by forming the PEN-PMN-PT ternary crystals. Higher Curie temperature was obtained as T_c ~291 °C for the 40PEN-13PMN-47PT crystals, together with larger coercive field (E_c ~17.6 kV/cm). The improvements in Curie temperature and coercive field of the PEN-PMN-PT crystals were attributed to the introduction of the PEN and the increasing of tetragonal phase. Moreover, a special absorption in the range 300–1800 nm and strong green UC emissions at the 980 nm excitation were obtained for the PEN-PMN-PT crystals.

Author Contributions: Conceptualization, Z.X.; methodology, W.Z.; formal analysis, W.Z.; investigation, W.Z.; resources, Z.X.; writing—original draft preparation, W.Z.; writing—review and editing, Z.X.; P.Y.; X.L.; W.L.; A.H.; Y.L. and Y.Z.; supervision, Z.X.

Conflicts of Interest: The authors declare no conflict of interest.

References

1. Zhang, S.; Li, F. High performance ferroelectric relaxor-$PbTiO_3$ single crystals: Status and perspective. *J. Appl. Phys.* **2012**, *111*, 2–27. [CrossRef]
2. Lee, H.J.; Zhang, S.; Luo, J.; Li, F.; Shrout, T.R. Thickness dependent properties of relaxor-$PbTiO_3$ ferroelectrics for ultrasonic transducers. *Adv. Funct. Mater.* **2010**, *20*, 3154–3162. [CrossRef] [PubMed]
3. Park, S.E.; Shrout, T.R. Ultrahigh strain and piezoelectric behavior in relaxor based ferroelectric single crystals. *J. Appl. Phys.* **1997**, *82*, 1804–1811. [CrossRef]
4. Lu, Y.; Jeong, D.Y.; Cheng, Z.Y.; Zhang, Q.M.; Luo, H.S.; Yin, Z.W.; Viehland, D. Phase transitional behavior and piezoelectric properties of the orthorhombic phase of $Pb(Mg_{1/3}Nb_{2/3})O_3$-$PbTiO_3$ single crystals. *Appl. Phys. Lett.* **2001**, *78*, 3109–3111. [CrossRef]
5. Noheda, B.; Cox, D.E.; Shirane, G.; Gao, J.; Ye, Z.G. Phase diagram of the ferroelectric relaxor $(1-x)$ $PbMg_{1/3}Nb_{2/3}O_3-xPbTiO_3$. *Phys. Rev. B.* **2002**, *66*, 340–351. [CrossRef]
6. Lebrun, L.; Sebald, G.; Guiffard, B.; Richard, C.; Guyomar, D.; Pleska, E. Investigations on ferroelectric PMN–PT and PZN–PT single crystals ability for power or resonant actuators. *Ultrasonics* **2004**, *42*, 501–505. [CrossRef] [PubMed]
7. Ye, Z.G. High-Performance Piezoelectric Single Crystals of Complex Perovskite Solid Solutions. *MRS Bull.* **2009**, *34*, 277–283. [CrossRef]
8. Yamashita, Y.; Harada, K.; Tao, T.; Ichinose, N. Piezoelectric properties of the $Pb(Sc_{1/2}Nb_{1/2})O_3$-$Pb(Mg_{1/3}Nb_{2/3})O_3$-$PbTiO_3$ ternary ceramic materials near the morphotropic phase boundary. *Integr. Ferroelectr.* **1996**, *13*, 9–16. [CrossRef]
9. Li, X.; Wang, Z.; Liu, Y.; He, C.; Long, X. A new ternary ferroelectric crystal of $Pb(Y_{1/2}Nb_{1/2})O_3$-$Pb(Mg_{1/3}Nb_{2/3})O_3$-$PbTiO_3$. *CrystEngComm* **2014**, *16*, 7552–7557. [CrossRef]
10. He, C.; Li, X.; Wang, Z.; Long, X.; Mao, S.; Ye, Z.G. Preparation and Characterization of New $Pb(Yb_{1/2}Nb_{1/2})O_3$-$Pb(Mg_{1/3}Nb_{2/3})O_3$-$PbTiO_3$ Ternary Piezo-/Ferroelectric Crystals. *Chem. Mater.* **2010**, *22*, 5588–5592. [CrossRef]

11.　Xing, J.T.; Du, P.; Luo, L.H.; Fang, Y.Q.; Zhao, X.Y.; Hu, X.B.; Chen, H.B. Growth and Characterization of Er^{3+}-doped Relaxor-based Ferroelectric Crystal PMNT. *J. Inorg. Mater.* **2015**, *30*, 135–140. [CrossRef]

12.　He, C.; Li, X.; Wang, Z.; Liu, Y.; Shen, D.; Li, T.; Long, X. Compositional dependence of properties of $Pb(Yb_{1/2}Nb_{1/2})O_3$-$Pb(Mg_{1/3}Nb_{2/3})O_3$-$PbTiO_3$ ternary ferroelectric crystals. *CrystEngComm* **2012**, *14*, 4513–4519. [CrossRef]

13.　Ying, L.; Fa-Chun, L.; Zhi-Gao, H.; Dong-Quan, S.; Xi-Fa, L. Preparation and Characterization of A New Ferroelectric Ternary Solid Solution $Pb(Lu_{1/2}Nb_{1/2})O_3$-$Pb(Mg_{1/3}Nb_{2/3})O_3$-$PbTiO_3$. *J. Inorg. Mater.* **2014**, *29*, 912–916. [CrossRef]

14.　Zhang, S.; Luo, J.; Hackenberger, W.; Shrout, T.R. Characterization of $Pb(In_{1/2}Nb_{1/2})O_3$-$Pb(Mg_{1/3}Nb_{2/3})O_3$-$PbTiO_3$ ferroelectric crystal with enhanced phase transition temperatures. *J. Appl. Phys.* **2008**, *104*, 064106. [CrossRef] [PubMed]

15.　Xu, G.; Chen, K.; Yang, D.; Li, J. Growth and electrical properties of large size $Pb(In_{1/2}Nb_{1/2})O_3$-$Pb(Mg_{1/3}Nb_{2/3})O_3$-$PbTiO_3$ crystals prepared by the vertical Bridgman technique. *Appl. Phys. Lett.* **2007**, *90*, 032901. [CrossRef]

16.　Luo, L.; Zhou, D.; Tang, Y.; Jia, Y.; Xu, H.; Luo, H. Effects of Mn doping on dielectric and piezoelectric properties of $0.71Pb(Mg_{1/3}Nb_{2/3})O_3$-$0.29PbTiO_3$ single crystals. *Appl. Phys. Lett.*. [CrossRef]

17.　Li, X.; Wang, Z.; He, C.; Liu, Y.; Long, X.; Han, S.; Pan, S. High piezoelectric response of a new ternary ferroelectric $Pb(Ho_{1/2}Nb_{1/2})O_3$-$Pb(Mg_{1/3}Nb_{2/3})O_3$-$PbTiO_3$ single crystal. *Mater. Lett.* **2015**, *143*, 88–90. [CrossRef]

18.　He, A.; Xi, Z.; Li, X.; Long, W.; Zhang, T.; Fang, P.; Zhang, J. Structure analysis and systematical electric properties investigation of PSN-PMN-PT single crystal. *J. Mater. Sci. Mater. Electron.* **2018**, *29*, 16004–16009. [CrossRef]

19.　Long, W.; Chu, X.; Xi, Z.; Fang, P.; Li, X.; Cao, W. Growth and property enhancement of Er^{3+}-doped $0.68Pb(Mg_{1/3}Nb_{2/3})O_3$-$0.32PbTiO_3$ single crystal. *J. Alloys Compd.* **2018**, *36*, 832–837. [CrossRef]

20.　Salaka, A.; Bushinsky, M.V.; Pushkarov, N.V.; Shilin, A.D.; Olekhnovich, N.M.; Vyshatko, N.P. A new ferroelectric $PbEr_{1/2}Nb_{1/2}O_3$. *Ferroelectrics* **1999**, *234*, 123–127. [CrossRef]

21.　Sternberg, A.; Shebanovs, L.; Yamashita, J.Y.; Antonova, M.; Livinsh, M.; Shorubalko, I. Structure and properties of high piezoelectric coupling $Pb(B'_{1/2}Nb_{1/2})O_3$-$PbTiO_3$ binary systems. *Ferroelectrics* **1999**, *224*, 137–144. [CrossRef]

22.　Ai, L.; Li, X.; Wang, Z.; Liu, Y.; He, C.; Li, T.; Chu, T.; Pang, D.; Tailorb, H.; Long, X. Preparation, structure, and electric properties of the $Pb(Zn_{1/3}Nb_{2/3})O_3$-$Pb(Yb_{1/2}Nb_{1/2})O_3$-$PbTiO_3$ ternary ferroelectric system ceramics near the morphotropic phase boundary. *J. Eur. Ceram. Soc.* **2013**, *33*, 2155–2165. [CrossRef]

23.　Xi, Z.; Hou, Z.; Li, X.; Fang, P.; Long, W. Study on structure and properties of $Pb(Sc_{1/2}Nb_{1/2})O_3$-$Pb(Mg_{1/3}Nb_{2/3})O_3$-$PbTiO_3$ ternary ceramics near morphotropic phase boundary. *Ceram. Int.* **2015**, *41*, S787–S791. [CrossRef]

24.　Xi, Z.; He, A.; Fang, P.; Li, X.; Long, W. Electric and optical properties of Er^{3+} and Er^{3+}/Yb^{3+} modified PSN-PMN-PT crystals. *J. Alloys Compd.* **2017**, *722*, 375–380. [CrossRef]

25.　Zeng, J.; Wei, Z.; Huang, Y.; Tsuboi, T.; Zheng, L.; Wang, S.; Li, G. NIR to Visible Up-conversion Luminescence of Er^{3+}-doped PMN-PT Transparent Ceramics. *J. Am. Ceram. Soc.* **2012**, *95*, 2573–2578. [CrossRef]

26.　Sun, Y.; Yang, Q.; Wang, H.; Zhang, Q.; Shao, Y. Preparation and mid-infrared 2.7 µm luminescence property of high content Er^{3+}-doped $(Y0.9La0.1)_2O_3$ transparent ceramics pumped at 980 nm. *Ceram. Int.* **2018**, *44*, 1812–1816. [CrossRef]

27.　Tikhomirov, V.K.; Rodríguez, V.D.; Méndez-Ramos, J.; Del-Castillo, J.; Kirilenko, D.; Tendeloo, G.; Moshchalkov, V. Optimizing Er/Yb ratio and content in Er–Yb co-doped glass-ceramics for enhancement of the up- and down-conversion luminescence. *Sol. Energy Mater. Sol. Cells* **2012**, *100*, 209–215. [CrossRef]